A new hybrid simulation integrating transient-state and steady-state models for the analysis of reversible DC traction power systems

Zhang, Gang; Tian, Zhongbei; Tricoli, Pietro; Hillmansen, Stuart; Liu, Zhigang

DOI:
10.1016/j.ijepes.2019.01.033

A new Hybrid Simulation Integrating Transient-state and Steady-state Models for the Analysis of Reversible DC Traction Power Systems

Gang Zhang[a], Zhongbei Tian[b*], Pietro Tricoli[b], Stuart Hillmansen[b], Zhigang Liu[c]

[a] School of Electrical Engineering, Beijing Jiaotong University, China
[b] Department of Electronic, Electrical and Systems Engineering, University of Birmingham, UK
[c] Beijing Electrical Engineering Technology Research Center, China

*Corresponding author: Zhongbei Tian, Email address: z.tian@bham.ac.uk

Abstract

This paper presents a new hybrid simulation method for reversible traction power supply systems (RTPSSs) supplied by four-quadrant converters (4QC). RTPSSs overcome several drawbacks of conventional DC electrification systems, such as wasting of braking energy, output voltage fluctuation, and low power factor at light load conditions. The paper introduces the system topology of a RTPSS and illustrates its advantages over standard DC systems. A hybrid simulation method is proposed to study the performance of the RTPSS taking into account the dynamics of multiple trains. This hybrid simulation integrates train motion, steady-state and transient-state models, and is able to evaluate both the system-level steady-state performance (voltage, current, power and energy) and the equipment-level transient-state performance (harmonics, ripple, power factor and stability). Structure and signals flow of this hybrid simulation system have been introduced, and the methodology of modeling has been presented. The validity and applicability of the proposed hybrid simulation method have been proved by a case study of a 10 km railway line with 6 substations. To date, no other work has accomplished the steady-state and transient-state study using a single integrated simulation.

Keywords: Traction power system; hybrid simulation; reversible substation; regenerative braking; system modeling;

1 Introduction

In a Traction Power Supply System (TPSS), several traction substations are powered by one or two main substations through three-phase medium voltage distribution networks (MVDN). The traction substations include transformers, diode rectifiers and switchgears. The merits of traditional TPSS are simplicity, robustness and low-cost. However, some obvious drawbacks exist：

- ✧ waste of regenerative braking energy. Especially when a small number of trains travel on the line, the regenerative braking energy cannot be reused within the DC network. It is usually dissipated by on-board braking resistors, causing temperature rise in tunnels and at the stations.
- ✧ fluctuation of DC voltage. Because of the unregulated characteristic of diode rectifiers, the output voltage has large fluctuations with variable loads.
- ✧ low power factor problem at AC grid interface. Studies indicate that it is usually caused by the equivalent capacitance of large amount of grid cables [1,2].

Some solutions have been proposed to overcome the above-mentioned drawbacks. In [3-5], thyristor-based inverters are introduced to feed the regenerative braking energy back to the MVDN. With the development of power semiconductors and converter control technology, IGBT inverters have been increasingly employed in TPSSs [6-12], which allows not only energy recovery, but also active power filtering [13-16]. Traction substations with IGBT inverters are called inverting substations or reversible substations. In order to reduce the voltage fluctuation of the DC network and improve the energy efficiency, the conventional diode rectifier is replaced by the controlled rectifiers in [8,9,17]. The installation of storage devices (such as super-capacitors or flywheels) [18-25] at substations or tracksides could be a good way to absorb the surplus regenerated energy and regulate DC voltage. However, compared with inverters, storage devices require more installation space, higher cost, and more safety constraints [17]. To improve power factor under light load condition, the traditional schemes based on Static Var Compensator (SVC) and Static Var Generator (SVG) are usually adopted in the TPSS [1,2,26-28]. The total capacity of SVGs in a typical line is normally several MVars.

The above solutions lead to an increase of equipment cost, system complications and increase of maintenance cost. Considering the excellent characteristics and fast development of Four-Quadrant Converters (4QC) [29,30], a reversible traction power supply system (RTPSS) equipped with pure high-power 4QC is recommended in this paper.

A simulation approach is indispensable to study and assess the performance of the RTPSS. According to the time duration and objectives of the simulations, three categories of models can be considered for the study of RTPSS: multi-train motion model, steady-state model (average static model) and transient-state model (instantaneous dynamic

model) [31,32]. Multi-train motion simulation is used to model train movement and traction power requirements [33]. Trains require different traction power while they travel along the power supply network. Kinetic train motion, track alignment, and operation timetable are usually considered in formulating the multi-train operation simulations [34]. Based on the steady-state mathematical model and iterative calculations, the steady-state simulation can be used to analyze power flows [20,35,36], evaluate energy consumption [31-33] and design the power supply system [4,37]. Steady-state simulations do not depend on specific software environment, and no control loops are required in the model. Moreover, the time step of steady-state simulations is relatively long, typically T_s = 1 s [38-40]. Steady-state simulations provide a global overview of the system during a whole day with short computational time [20]. Transient-state simulations study the control and dynamic performance during a shorter time step, typically 20ms or less). Transient-state simulations, which are based on the electrical circuit model and closed-loop control, can be used instead to verify control algorithms, evaluate power quality, and analyze system stability. Transient-state simulations usually rely on the specific simulation software or tools, such as Simulink, Psim, and Pspice. Transient-state simulations are mainly used in equipment-level simulations [41,42] or occasionally in short-circuit simulations [43].

In most previous studies, train motion simulation, steady-state simulation and transient-state simulation are carried out separately. The study of multi-train motion has not considered the capacity of TPSS. The study of steady-state power flow has not considered the response ability of the control loops and cannot provide information on instantaneous waveforms, harmonic content, ripple and so on. The study of the transient-state simulation usually focuses on limited devices during short time, which cannot be used to study the system performance. Therefore, the previous studies lead to inefficiency on the system study and performance evaluation. Firstly, it is time-consuming to build these three simulation models on different software environment and platforms. Secondly, it has not realized data interaction and sharing between different simulations. In this paper, a hybrid simulation method integrating steady-state and transient-state models is proposed to achieve a combination of train motion, steady-state and transient-state simulation. It can be used as an efficient tool for the study of the power supply system based on controllable converters and accomplish the verification and assessment of the system performance with consideration of multi-train operations.

This paper is structured as follows; the section 2 introduces the system schematic and advantages of the RTPSS, as well as the topology of the reversible traction substation. In section 3, the structure of the hybrid simulation system is proposed, and the modeling of train motion, steady-state and transient-state are illustrated. In section 4, a case study is carried out to verify the function and validity of the proposed hybrid simulation method. The conclusions are presented in section 5.

2 Principle of a RTPSS

2.1 System schematic

A RTPSS normally employs controllable converters to achieve a flexible energy conversion. The topology of a typical RTSS is shown in Figure 1. With 4QCs, the energy can be transmitted between AC and DC in both directions and the power factor is adjustable.

The advantages of the proposed system are demonstrated below:

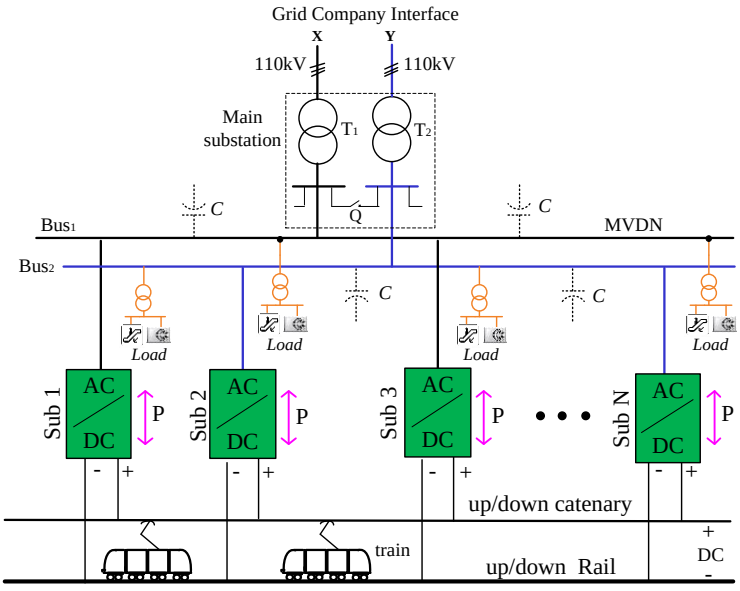

Figure 1 Topology of a typical RTPSS

1） The regenerative braking energy of the trains can be inverted back to the AC grid for reusing, as shown in Figure 2a. 4QCs work in the inverter mode. Thereby it can effectively reduce the energy consumption of the entire power supply system, reduce the mechanical wear of the brake shoes and avoid temperature rise of the tunnels;

2） The trains are powered by controllable substations, as shown in Figure 2b. 4QCs work in the rectifier mode. The DC output voltage can keep constant through closed loop control. Therefore, the power supply quality can be significantly improved in terms of voltage fluctuation, and the distance between adjacent traction substations can be extended;

3） Reactive power compensation can be realized by generating required opposite reactive power and injecting into grid, as shown in Figure 2c, replacing the traditional SVG to ensure high power factor of the AC grid interface;

4） Anti-icing or de-icing functions can be implemented on the electrification line with an appropriate control of the substations, as shown in Figure 2d. Sub1 works as an inverter and Sub3 works as a rectifier. Energy circulation through two substations, AC grid and catenary can be made, ensuring safety of the catenary and pantograph in extreme weather conditions.

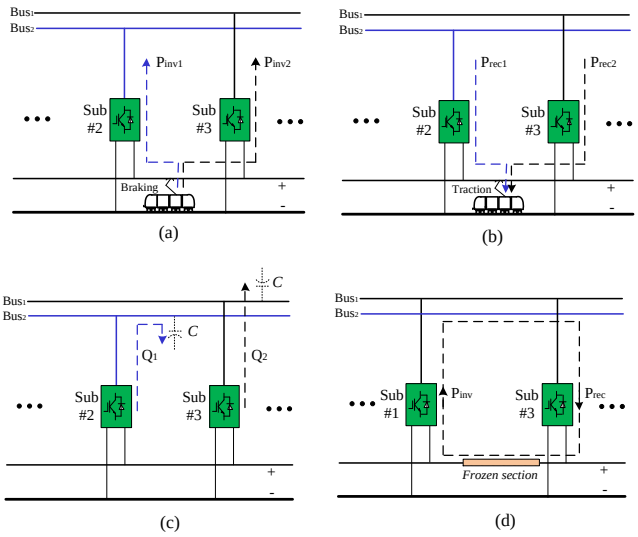

Figure 2 Typical functions of the RTPSS

2.2 Reversible traction substations

Each traction substation in RTPSS is mainly composed of two identical 4QC units, as shown in Figure 3. They are connected in parallel at both AC side and DC side, which not only expands the capacity of the system, but also improve the reliability of the power supply system in case of failures. With this topology, the carrier phase-shifted PWM (CPS-PWM) can be used to reduce the harmonics of the current drawn from the AC grid.

Each 4QC unit includes one medium voltage breaker (H_1/H_2), one transformer (RT_1/RT_2), one high-power 4QC ($4QC_1$/$4QC_2$), one DC breaker (Q_1/Q_2) and one isolating switchgear (G_1/G_2).

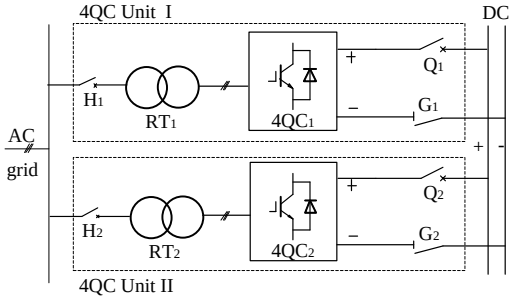

Figure 3 Topology of 4QC-based reversible traction substation

3 Hybrid simulation and modeling

3.1 Hybrid simulation scheme

The hybrid simulation method proposed in this paper is carried out on the software platform MATLAB, in order to combining the large-time scale of the steady-state simulation and the small-time scale of transient-state simulation. The steady-state simulation is implemented through M file in MATLAB, meanwhile the transient-state simulation is accomplished by Simulink in MATLAB.

Figure 4 shows the simplified network topology of the RTPSS. Considering that the up and down rails are bound together every 200-300 meters, they can be assumed to have the same potential. With this assumption, the rail resistance can be included in the overhead contact line [38,39]. Figure 4 will be used to construct the network node admittance matrix $\boldsymbol{Y}$ which is required in the power flow solver.

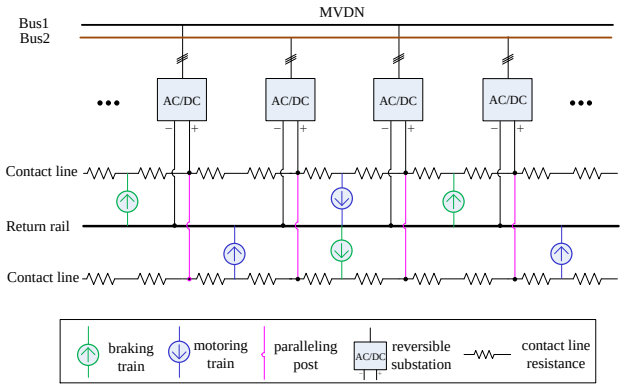

Figure 4 Simplified network topology of the RTPSS

Figure 5 shows the structure of the proposed hybrid simulation system with details on the data and signal flow. The whole simulation system is mainly divided into three parts: train motion simulation, steady-state simulation and transient-state simulation. Train motion simulation is developed considering train parameters, driving strategies, speed limits and route data. Then the real-time location $S_i(t)$ and electrical power demand of trains $P_i(t)$ is calculated and used as input data for both the steady-state simulation and the transient-state simulation. The steady-state simulation is formulated from the mathematic model

of RTPSS. The network admittance matrix is constructed and then the voltage and current of each node in the system is obtained through iterative calculation. The solution of the equation of the model provides other useful data, such as the power curve, energy consumption and system loss. The state variables of the system, i.e. the voltage and current of each node, are indicated as $x_i^{ss}(t)$. The value of $x_i^{ss}(t)$ is sent to the transient-state simulation as the initial values of these state variables.

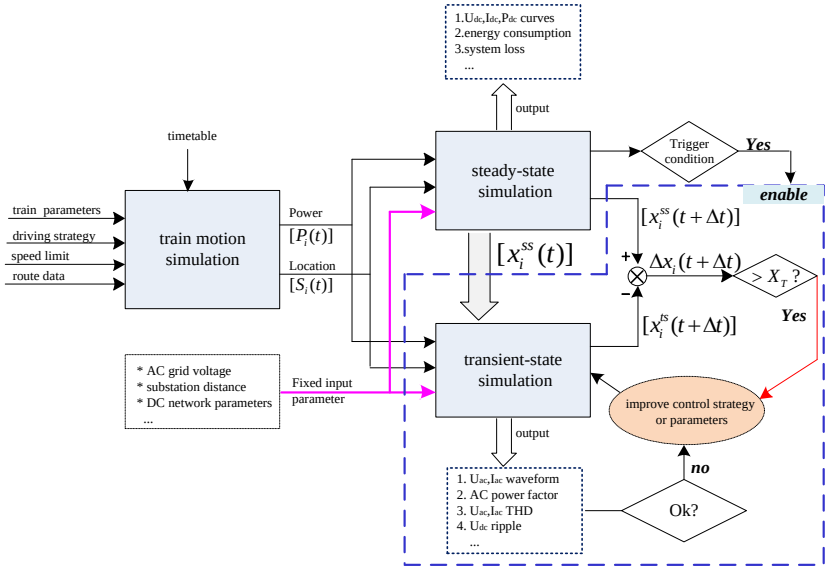

Figure 5 Structure and signal flow of the proposed hybrid simulation system

The electrical parameters and control laws of the equipment and components in the RTPSS can be accurately described in the model, by means of which the transient-state value of each node, such as waveforms, total harmonic distortion (THD), power factor and ripple, can be obtained. So, the transient-state simulation is similar to a microscope and provides important additional information to the steady-state simulation. In addition, the dynamic performance and stability of the system can be verified by comparing the value of selected state variables calculated by steady-state simulation and by the transient-state simulation. In Figure 5, $x_i^{ss}(t + \Delta t)$ is the steady-state value and $x_i^{ts}(t + \Delta t)$ is the transient-state value at the same time. Theoretically, the deviation $\Delta x_i(t + \Delta t)$ between $x_i^{ss}(t + \Delta t)$ and $x_i^{ts}(t + \Delta t)$ should be very small. If the condition shown in (1) is satisfied, where X_T is the defined threshold value, it means the expected steady-state value does not match well with the transient-state value. So, some improvements of the control strategy or control parameters (such as closed-loop Kp, Ki) should be considered.

$$\begin{cases} \Delta x_i(t + \Delta t) = x_i^{ss}(t + \Delta t) - x_i^{ts}(t + \Delta t) \\ |\Delta x_i(t + \Delta t)| > X_T \end{cases} \quad (1)$$

The transient-state simulation process is time-consuming due to its sophisticated model and small time-step, so it should be launched manually at specific times, or be enabled by software through certain trigger conditions. In this paper, the variation of substation output power $\Delta P_{sub\_i}^{ss}$ is selected as a trigger condition, as shown in (2):

$$\begin{cases} \Delta P_{sub\_i}^{ss}(t + \Delta t) = |P_{sub\_i}^{ss}(t + \Delta t) - P_{sub\_i}^{ss}(t)| \\ \Delta P_{sub\_i}^{ss}(t + \Delta t) > P_T \end{cases} \quad (2)$$

where $P_{sub_i}^{ss}(t)$ is the substation output power derived from steady-state simulation, P_T is the trigger threshold value.

Figure 6 shows the relationship between steady-state and transient-state simulation. The time step of the steady-state simulation is set to 1 s ($T_s^{ss} = 1\ s$), which is equal to the total simulation period of the transient-state simulation for one cycle. The time step of the transient-state simulation is set to 5 μs (T_s^{ts}=5 μs). $[x_i^{ss}(0), x_i^{ss}(1), x_i^{ss}(2), \ldots, x_i^{ss}(n)]$ denote the steady-state value of state variable x_i at t = 0, 1, 2, 3,…, n. In addition, [$x_i^{ts}(2)$, $x_i^{ts}(2.000005)$, $x_i^{ts}(2.000010)$,…, $x_i^{ts}(3)$] denote the transient-state value of state variable x_i at t = 2, 2.000005, 2.000010,…, 3.

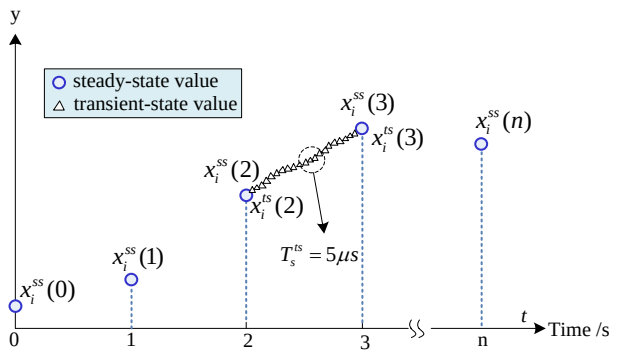

Figure 6 Relationship between steady-state and transient-state

It is assumed that the transient-state simulation is

launched manually at $t = 2$ s. The steady-state value of state variable x_i at $t = 2$ s is passed to the transient simulation as the initial values, as shown in (3):

$$x_i^{ts}(2) = x_i^{ss}(2) \tag{3}$$

After that, the transient-state simulation is launched, adopting the time step of 5 μs. At the end of the transient-state simulation, the value $x_i^{ts}(3)$ at $t = 3$ s is obtained and the deviation $\Delta x_i(3)$ can be calculated, as shown in (4):

$$\Delta x_i(3) = x_i^{ss}(3) - x_i^{ts}(3) \tag{4}$$

3.2 Train motion modeling

The forces on a motoring train along an uphill slope are shown in Figure 7.

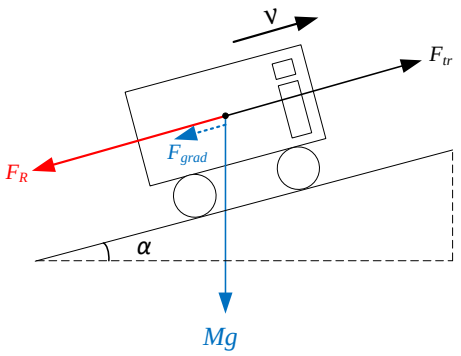

Figure 7 Forces on a motoring vehicle

The train tractive effort (F_{tr}) applied to a train is used to move the train against the motion resistance (F_R) and gravitational forces (F_{grad}). The train kinematic model can be expressed by the Newton's second law of motion in (5) [38]:

$$M_{eff}\frac{\mathrm{d}^2 s}{\mathrm{d}t^2} = F_{tr} - F_R - F_{grad} \tag{5}$$

where M_{eff} denotes the effective mass including the rotary allowance, s denotes the vehicle position along the track, t is the time.

The total motion resistance including the rolling resistance and curvature resistance can be obtained from (6) [38]:

$$F_R = (A + Bv + Cv^2) + \frac{D}{r} \tag{6}$$

where A, B and C are Davis coefficients, D is curvature resistance constant, v is the train speed and r is the curve radius [39].

The gravitational force is calculated according to the slope angle α in (7).

$$F_{grad} = Mg\sin(\alpha) \tag{7}$$

The train mechanical power, P_{me}, is given in (8).

$$P_{me} = F_{tr} \times v \tag{8}$$

The mechanical power is positive when the train is motoring and negative when the train is braking.

The traction power requirement, P_{req}, is given in (9):

$$P_{req} = \begin{cases} \dfrac{P_{me}}{\eta} & ,if\ P_{me} \geq 0 \\ P_{me} \times \eta & ,if\ P_{me} < 0 \end{cases} \tag{9}$$

where η denotes the efficiency of traction chain.

With the timetable information, the position of the trains and their traction power requirements at each instant are collected and used as the inputs for the steady-state simulation and the transient-state simulation.

3.3 Steady-state modeling

Steady-state simulation plays an important role in system-level research, such as power flow distribution analysis, equipment capacity configuration, and system energy consumption assessment. In addition, the output of the steady-state simulation is used to set the initial state of the transient-state simulation.

3.3.1 Modeling of 4QCs

In the RTPSS, the 4QC is the core equipment to supply the trains and recover the surplus regenerative braking energy that cannot be absorbed by other motoring trains. The most notable features of 4QC are bidirectional power flow and controllable DC characteristic [29], shown in Figure 8.

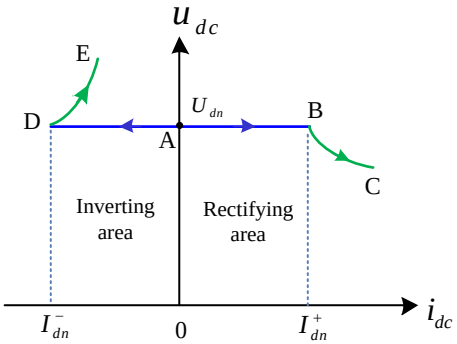

Figure 8 DC characteristic

In Figure 8, the rectifying area is located in the first quadrant (right), and the inverting area is located in the second quadrant (left). AB and AD are defined as constant voltage curve. The 4QC is equivalent to an ideal voltage source, and the corresponding maximum operating current are I_{dn}^+ and I_{dn}^-, respectively. BC and DE are defined as constant power curves, and the 4QC is equivalent to ideal power source. Regarding the curve BC, due to the limitation of rectifying power P_{rec}^{max}, the 4QC DC output voltage will rapidly drop with the increase of the train traction power, following an hyperbolic law. Considering the curve DE,

because of the limitation of inverting power P_{inv}^{max}, the 4QC DC output voltage will rapidly rise with the increase of the train braking power, following a hyperbolic law.

The DC voltage characteristics of 4QC can be expressed by (10):

$$u_{dc} = \begin{cases} U_{dn},\ if\ I_{dn}^{-} \le i_{dc} \ll I_{dn}^{\mp} \\ \dfrac{P_{rec}^{max}}{i_{dc}},\ if\ \ I_{dn}^{+} < i_{dc} \\ \dfrac{P_{inv}^{max}}{i_{dc}},\ if\ i_{dc} < I_{dn}^{-} \end{cases} \tag{10}$$

When a train is motoring, it will not get power from other substations until the adjacent two substations reach the maximum power P_{rec}^{max}. A similar situation occurs when the train brakes.

3.3.2 Modeling of the trains

The train electrical system mainly includes a traction converter and an auxiliary inverter for the hotel loads, such as controllers, air conditioners, heaters and lamps.

As mentioned before, the traction power requirement changes with the position and velocity of the train and it is calculated by the train motion simulation. So, the traction converter can be modeled as a time-varying power load. Instead, the power of the auxiliary inverter does not change significantly over a journey. So, the auxiliary converter can be modeled as a constant power load. Therefore, the whole train can be modeled as shown in Figure 9 and the electrical power of the train can be expressed by equation (11):

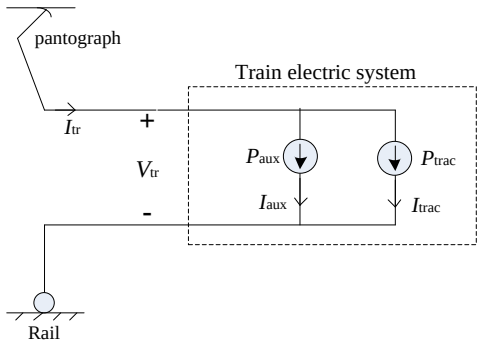

Figure 9 Electrical model of a train

$$\begin{cases} P_{tr} = P_{trac} + P_{aux} \\ P_{tr} = V_{tr} \times I_{tr} \end{cases} \tag{11}$$

where P_{trac} and P_{aux} represent the traction power and auxiliary power of the train, and V_{tr} and I_{tr} represent the voltage and current of the train.

Equation (11) highlights that the actual traction power depends on the train voltage. When the train voltage is too low or too high, a linear derating of the power is usually adopted to avoid overcurrent or overvoltage of the traction converter. Figure 10 shows the traction power limitation curve of the train [44].

When the train is in traction mode ($P_{trac} > 0$), the limit power P_{t_lim} can be expressed by (12) .

$$P_{t\_lim} = \begin{cases} \dfrac{V_{tr} - V_1}{V_2 - V_1} \cdot P_{t\_max},\ V_1 < V_{tr} < V_2 \\ P_{t\_max},\ V_2 < V_{tr} < V_4 \\ \dfrac{V_6 - V_{tr}}{V_6 - V_4} \cdot P_{t\_max},\ V_4 < V_{tr} < V_6 \\ 0,\ V_{tr} < V_1\ or\ V_{tr} > V_6 \end{cases} \tag{12}$$

where P_{t_max} is the maximum traction power. V_2 and V_4 are the curve breaks of low voltage and high voltage respectively, which means the maximum traction power is available only when the train voltage is higher than V_2 and lower than V_4.

When the train is in braking mode ($P_{trac} < 0$), the limit power P_{b_lim} can be expressed by (13) .

$$P_{b\_lim} = \begin{cases} \dfrac{V_{tr} - V_1}{V_3 - V_1} \cdot P_{b\_max},\ V_1 < V_{tr} < V_3 \\ P_{b\_max},\ V_3 < V_{tr} < V_5 \\ \dfrac{V_6 - V_{tr}}{V_6 - V_5} \cdot P_{b\_max},\ V_5 < V_{tr} < V_6 \\ 0,\ V_{tr} < V_1\ or\ V_{tr} > V_6 \end{cases} \tag{13}$$

where P_{b_max} is the maximum braking power. V_3 and V_5 are the curve breaks of low voltage and high voltage respectively, which means the maximum braking power is available only when the train voltage is higher than V_3 and lower than V_5.

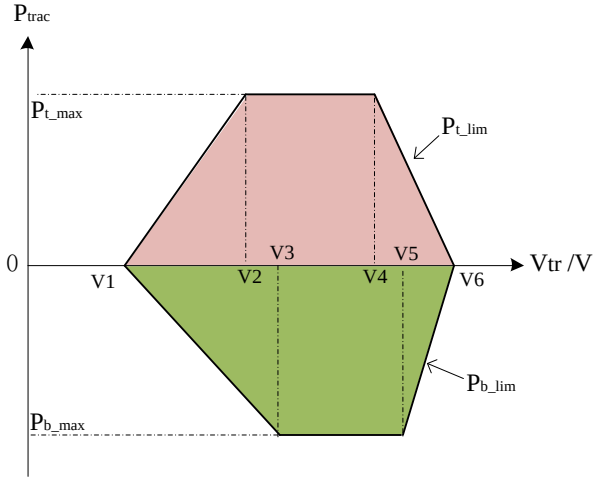

Figure 10 Traction power limitation curve of the train

3.3.3 Power flow solver

A power flow solver has been developed to analyze the railway power system for steady-state operations. According to the results from the train motion simulation, all the network information is gathered at each time step. Thus, the power requirements of the different trains are known. The trains are modeled as voltage-controlled current

sources, as shown in (14):

$$I_{tr\_n} = \frac{P_{tr\_n}}{V_{tr\_n}} \tag{14}$$

According to the location of train in the network, the conductor resistance between the train and the substations can be calculated by (15), where ρ the resistivity of the contact is line and l_{c_n} denotes the length of each conductor.

$$R_{c\_n} = \rho \times l_{c\_n} \tag{15}$$

The network node admittance matrix $\boldsymbol{Y}$ can be formulated using the chain circuit rules [44].

Current injection iterative method is used to solve the power flow [40]. The initial voltage of each train is set to substation no-load voltage according to (16). Thus, the current of each train at next iteration can be calculated and the nodal voltages of the next step are updated in (17). By iterative computation, nodal voltages converge to steady values. The solution then provides the voltage and current for each train on the line.

$$V_{tr\_n}^{(0)} = V_{sub} \tag{16}$$

$$\begin{cases} I_{tr\_n}^{(\mathrm{i}+1)} = \dfrac{P_{tr\_n}}{V_{tr\_n}^{(\mathrm{i})}} \\ \boldsymbol{V}^{(\mathrm{i}+1)} = \boldsymbol{Y}^{-1} \times \boldsymbol{I}^{(\mathrm{i}+1)} \end{cases} \tag{17}$$

3.4 Transient-state modeling

3.4.1 Modeling of AC cable

Centralized power supply mode is widely used in the urban traction power supply system, as shown in Figure 1. A 35 kV cable is used to connect the main substation to each traction substation. A 110 kV cable is used to connect the main substation to the grid. Capacitive reactive power generated by 35 kV and 110 kV cables lead to low power factor at the grid interface, especially when system load is light (the active power consumed is very small).

In order to assess the influence of cable's equivalent parameters on system performance for the transient-state simulations, the π-type equivalent circuit is adopted in this paper, as shown in Figure 11.

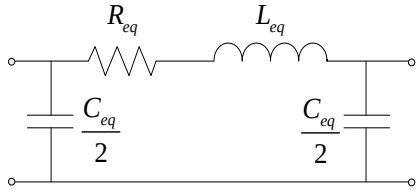

Figure 11 π-type equivalent circuit for AC cable

It is assumed that r is the cable resistance per unit length (Ω/km), l is the cable inductance per unit length (H/km), and c is the cable capacitance per unit length (F/km). So, the equivalent resistance, inductance and capacitance for a length l_{sec} of medium-voltage cable can be expressed by equation (18).

$$\begin{cases} R_{\mathrm{eq}} = r \times l_{sec} \\ L_{\mathrm{eq}} = l \times l_{sec} \\ C_{\mathrm{eq}} = c \times l_{sec} \end{cases} \tag{18}$$

3.4.2 Modeling of 4QC

（1）Main circuit

The main circuit of 4QC is shown in Figure 12.

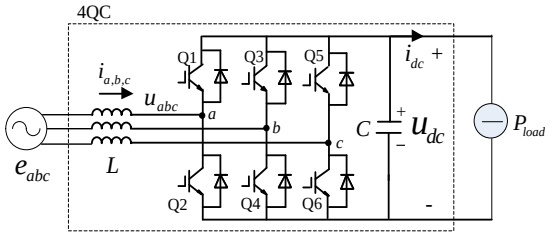

Figure 12 Main circuit of 4QC

In Figure 12, L is the AC filter inductance, C is the capacitance of DC-Link, a/b/c is the midpoint of each half-bridge, u_{dc} *and* i_{dc} is the DC voltage and current of 4QC respectively, e_{abc} is the voltage of AC source, P_{load} is the DC load.

According to KVL law, the mathematic model of the 4QC can be given (19):

$$\begin{cases} e_a = L\dfrac{di_a}{dt} + u_a \\ e_b = L\dfrac{di_b}{dt} + u_b \\ e_c = L\dfrac{di_c}{dt} + u_c \end{cases} \tag{19}$$

where

e_a, e_b, e_c denote the phase voltage of the power source;

i_a, i_b, i_c denote the current of each phase;

$u_a, \mathrm{u_b}, \mathrm{u_c}$ denote the phase voltage of 4QC;

（2）AC current control scheme

Since the three-phase current of 4QC are AC variables, the steady state error will not be zero with conventional PI controllers. So, the control strategy based on *dq* rotating frame is employed in this paper. Using the transformation matrix, equation (20) can be written as:

$$\begin{cases} e_d = L\dfrac{di_d}{dt} - \omega L i_q + u_d \\ e_q = L\dfrac{di_q}{dt} + \omega L i_d + u_q \end{cases} \tag{20}$$

The closed-loop control block diagram for AC current of 4QC is shown in Figure 13.

AC current control is used to improve the THD, power factor and dynamic response of 4QCs.

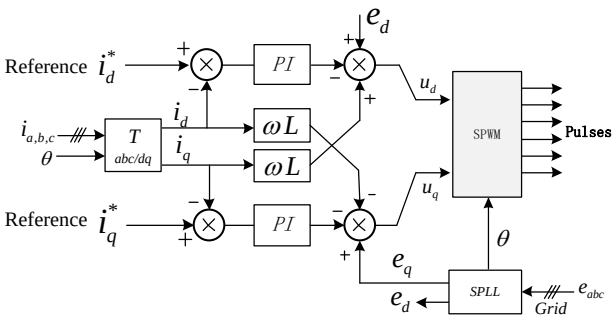

Figure 13 Closed-loop control block diagram

（3）DC voltage control scheme

Since there are two 4QC units in a traction substation, the DC voltage control scheme in Figure 14 is proposed. This produces the expected DC characteristic shown in Figure 8 and ensures equal sharing of the load between the two 4QCs.

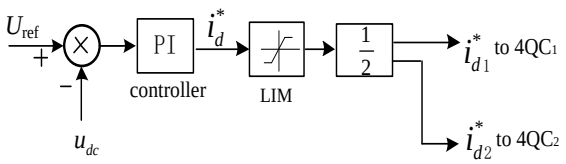

Figure 14 DC voltage control scheme

3.4.3 Modeling of the trains

In the transient-state simulation, the trains are also modeled as a controllable power source to reduce the system computation burden. This has been implemented in practice with a controllable current source block, as shown in Figure 15, where P_{tr} is the total power demand of the train, considering the power limitation shown in Figure 10. I_{tr} is then used as the current reference of the inner controllable current source. The current I_{tr} can be calculated by equation (21).

$$I_{\mathrm{tr}} = \frac{P_{tr}}{V_{tr}} \tag{21}$$

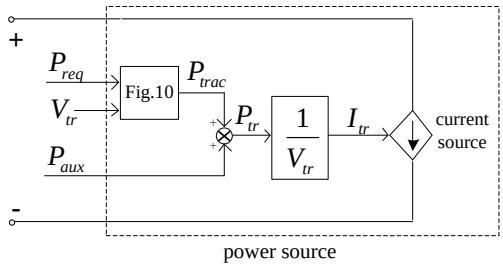

Figure 15 Power source model of the train

4 Case study

The objective of this section is to validate the function performance of the proposed hybrid simulation for a RTPPS.

4.1 Simulation parameters

The case study refers to a typical light railway line, which covers a length of 10 km and contains 6 substations. All substations are 4QC-based reversible substations with nominal voltage of 850 V.

The other simulation parameters are shown in Table 1.

Table 1 Parameters in the case study

Operation parameters	Value
Headway [s]	120
Terminal turnaround time [s]	300
DC network Parameters	Value
Contact line resistivity [mΩ/km]	20
Train Parameters	Value
Train mass including passengers [ton]	222.8
Motion resistance [kN]	$3.48+0.04025\times v$ $+0.0006575\times v^2$
Maximum operation speed [km/h]	80
Maximum traction power [kW]	3000
Maximum tractive effort [kN]	300
Maximum braking power [kW]	-3000
Maximum braking effort [kN]	-300
Auxiliary power [kW]	45
AC cable Parameters	Value
Resistance per unit length [Ω/km]	0.158
Inductance per unit length [mH/km]	0.287
Capacitance per unit length [μF/km]	0.156
4QC parameters	Value
Rated capacity [kW]	2000
AC rated voltage [V]	450
DC rated voltage [V]	850
AC filtering inductor L [μH]	150
DC-Link capacitor [mF]	36
Switch frequency fs [kHz]	2000
PWM method	CPS-SPWM

4.2 Hybrid simulation analysis

4.2.1 Train motion simulation

A train operation timetable is shown in Figure 16. The first upward train departs at 0s and arrives at the other terminal at 942s. The first downward train departs at 1242s and arrives at the other terminal at 2209s. When the first downward train arrives at the other end of the line, the number of trains simultaneously travelling on the network is the maximum. The timetable repeats every 120 s, according to the headway given in Table 1.

Figure 17 shows a train's speed and power profile from the train motion simulation.

According to Figure 5, the power and location of each train is transferred to the steady-state and transient-state simulations

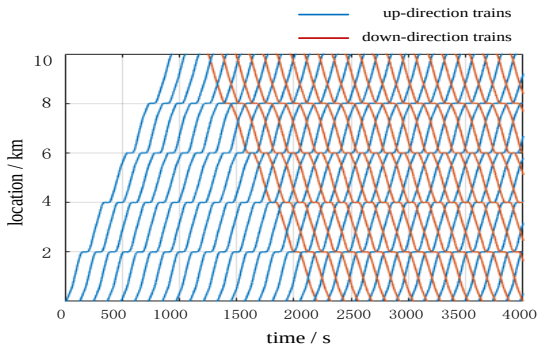

Figure 16 Timetable

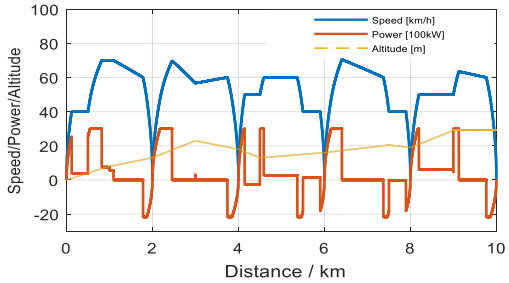

Figure 17 Speed and power profile of a train

4.2.2 Steady-state simulation results

The results of the steady-state simulation for the timetable of Figure 16 are shown in Table 2. It can be seen that the power supplied by Sub3 is the highest, while the power recovered from Sub6 is the highest. The energy supplied and recovered by each substation for one day operation (18h) is also presented in Table 2.

The instantaneous powers of Sub1 and Sub5 from 0s to 4000s are shown in Figure 18. Both the instantaneous maximum value and average value of the power will give guidelines for the design of the substation capacity.

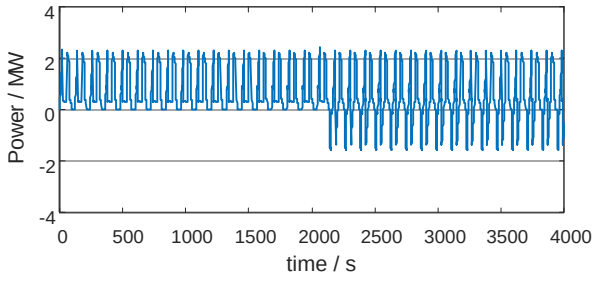

(a) Sub1

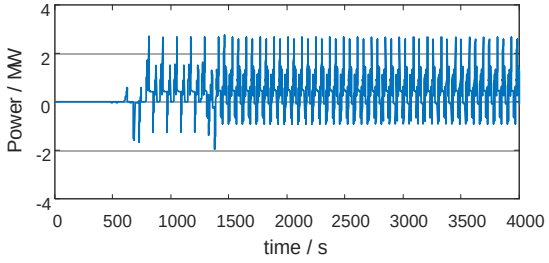

(b) Sub5

Figure 18 Instantaneous powers of Sub1 and Sub5

Table 2 Substation operation results

NO.	$P^{max}_{supplied}$ [MW]	$P^{mean}_{supplied}$ [MW]	$E_{supplied}$ [MWh]	$P^{max}_{recovere}$ [MW]	$P^{mean}_{recovere}$ [MW]	$E_{recovere}$ [MWh]
Sub1	2.30	0.63	11.27	1.56	0.25	4.45
Sub2	2.75	0.79	14.30	1.81	0.23	4.08
Sub3	3.42	0.80	14.35	1.69	0.30	5.38
Sub4	3.17	0.77	13.85	1.67	0.17	3.08
Sub5	2.71	0.59	10.58	1.89	0.07	1.32
Sub6	2.74	0.61	11.04	1.93	0.30	5.46

The train power and voltage from the steady-state simulation are shown in Figure 19 for a time window of 10 seconds. It can be seen that the maximum and minimum train voltage reach 861 V and 832 V, respectively. However, the voltage fluctuation in conventional TPSS is normally from 750V to 950V [38]. So the voltage fluctuation in RTPSS is obviously reduced in comparison to conventional TPSS.

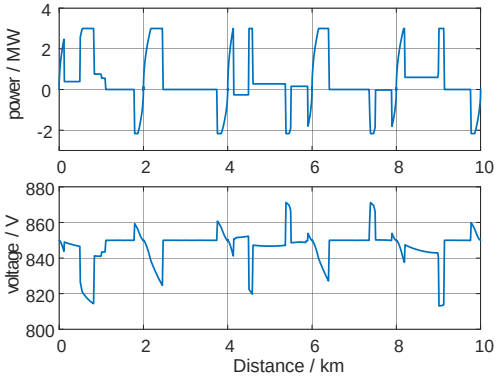

Figure 19 Train power and voltage from steady-state simulation

4.2.3 Transient-state simulation results

The AC side voltage and current waveforms of Sub1 and Sub5 at time 3029 seconds are shown in Figure 20 and Figure 21 respectively.

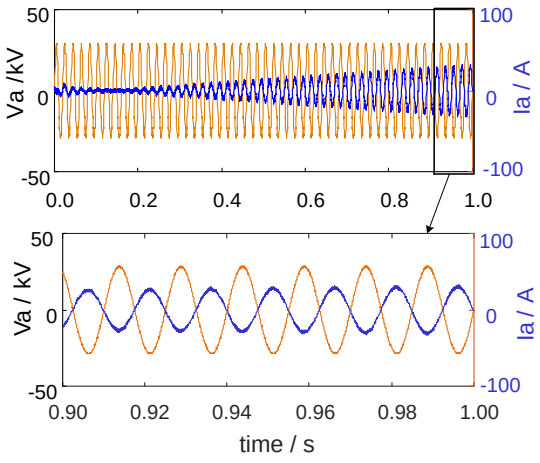

Figure 20 AC side voltage and current waveforms of Sub1

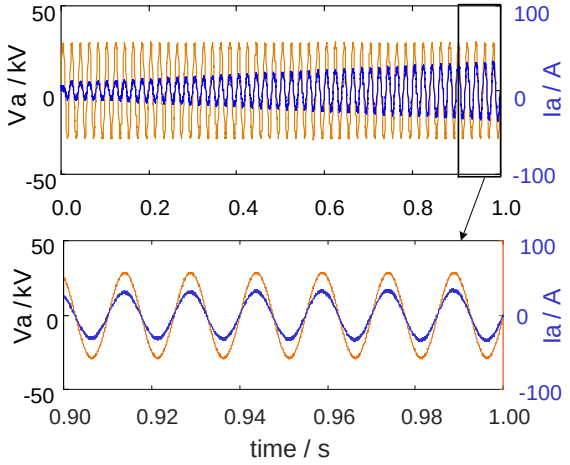

Figure 21 AC side voltage and current waveforms of Sub5

It can be seen that Sub1 works in inverter-mode and the current amplitude is increasing rapidly. Sub5 works instead in rectifying state, and the current amplitude is also increasing.

In order to quantitatively estimate the voltage and current harmonics generated by the reversible substation, the FFT analysis tools can be used. For instance, current spectrums of the Sub1 and Sub5 within 20ms at t=3029.98s are shown in Figure 22. It can be seen that the current THD reaches 4.18% and 3.80% respectively. Due to CPS-PWM, the characteristic harmonics of AC current are nearby 4000Hz. They are easy to be filtered by the equivalent capacitance of the MVDN.

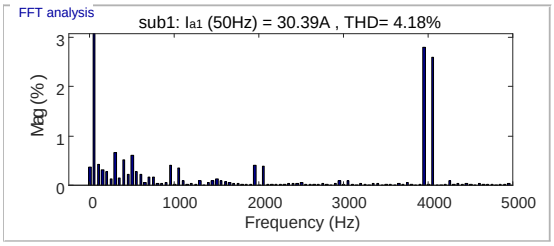

(a) Sub1

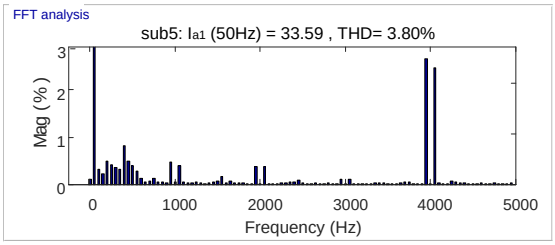

(b) Sub5

Figure 22 AC current spectrums of Sub1 and Sub5

The DC voltage and current waveforms of Sub1 and Sub5 are shown in Figure 23. It can be seen that the DC output current of Sub1 decreases rapidly and turns negative. The DC output current of Sub5 is instead increasing. The DC voltage is firmly kept nearby 850V and it is worth mentioning that the transient-state simulation allows a detailed calculation of the DC voltage ripple.

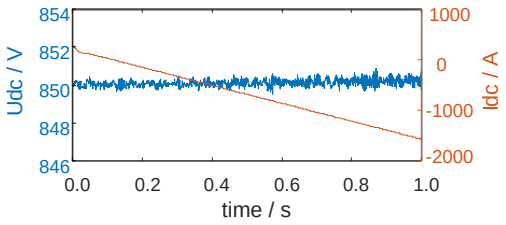

(a) Sub1

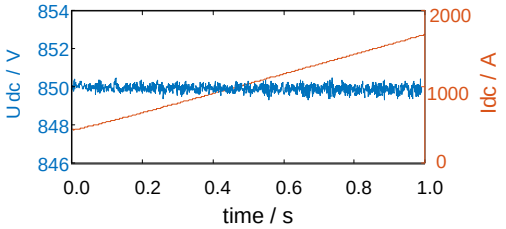

(b) Sub5

Figure 23 DC side voltage and current of Sub1 and Sub5

The DC voltage and current of the trains can easily be obtained to assess their working situation. Figure 24 shows the voltage and current waveforms of the upward train No.14 and downward train No.1 at t =3029 seconds.

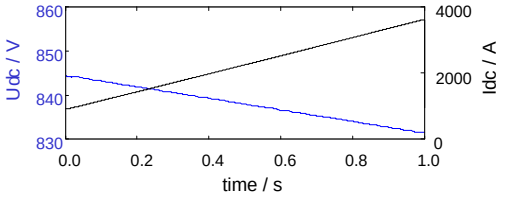

(a) up-direction train 14

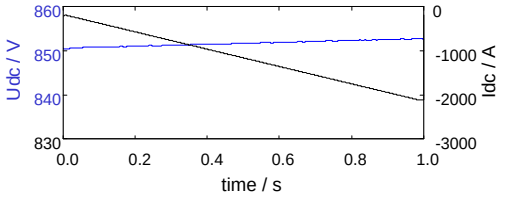

(b) down-direction train 1

Figure 24 Voltage and current of the up train 14 and down train 1

In addition, the power factor of the AC grid network at any instant of time can be calculated by the transient-state simulation. The simulation results show that the power factor at the input point of main substation is as low as 0.5 when there are no trains on the line and only auxiliary equipment are in use (supposing 50 kW/substation). When a 3-km-long 110 kV cable is also considered, the power factor seen by the grid is as low as 0.1. The total capacitive reactive power at the point of connection to the grid is about 2200 kVA. When every reversible substation generates 700 kVA of reactive power, the power factor at grid interface can be increased to more than 0.95, removing the need for traditional SVGs.

4.2.4 Comparison of simulation results

According to subsection 3.1, the initial value of the state

variables of the transient-state simulation comes from the steady-state simulation. Meanwhile, when the transient-state simulation has finished, the final value of the state variables should be close enough to the corresponding value calculated by steady-state simulation. Otherwise, it indicates that the dynamic performance of 4QCs cannot meet the demand of the railway system leading to oscillations and/or instabilities. Then the control strategy or the parameters of the 4QCs should be improved.

The DC output current i_{dc} of each substation is chosen as a state variable, and the trigger condition of transient-state simulation is set to $P_T = 4MW$. That means when the variation of a substation output power $\Delta P^{ss}_{sub\_i}$ exceeds 4MW, the transient-state simulation will be triggered automatically.

Two sets of transient-state simulation results are selected randomly, and then compared with results of the steady-state simulation, as shown in Table 3. The times t_1 and t_2 denote the start and end time of the transient-state simulation, respectively. The quantity Δi_{dc} denotes the variation of steady-state value from t_1 to t_2, while the quantity $Err_i = i^{ss}_{dc}(t_2) - i^{ts}_{dc}(t_2)$ denotes the deviation between the steady-state simulation and transient-state simulation at t_2. It can be seen from Table 3 that Err_i is related to Δi_{dc}. When Δi_{dc} is large, Err_i is usually also large. For example, for Δi_{dc}=-5185 A at Sub4 in the time interval [3025, 3026], it is Err_i=-177A. This is reasonable because the regulation process will last longer when the output power of the substation has a sudden change. The error Err_i can be reduced by improving the control strategy or control parameters of reversible converter but it cannot be completely eliminated. Considering that the substation rated capacity is 4 MW, a maximum current deviation of 208 A in the time interval [3075, 3076] accounts for 5.1% of the rated output current.

In addition, if a large Err_i is found at one substation, Err_i of adjacent substations is also relatively large due to the interaction between the substations. However, the algebraic sum of all substations Err_{sum} is close to zero as shown in (22).

$$Err_{sum} = \sum_{i=1}^{n} Err_i \approx 0 \qquad (22)$$

where Err_i represents the deviation value of a substation.

Table 3 Simulation results in [A]

time	[t1,t2] = [3025,3026]					
item	$i^{ss}_{dc}(t_1)$	$i^{ss}_{dc}(t_2)$	$i^{ts}_{dc}(t_1)$	$i^{ts}_{dc}(t_2)$	Δi_{dc}	Err_i
Sub1	488	515	488	531	27	-16
Sub2	2040	2142	2040	2088	102	54
Sub3	1191	186	1191	144	-1005	42
Sub4	3733	-1452	3733	-1275	-5185	-177
Sub5	991	296	991	212	-695	84
Sub6	246	253	246	242	7	11
Sum	8690	1940	8690	1942	-6750	-2
time	[t1,t2] = [3075,3076]					
item	$i^{ss}_{dc}(t_1)$	$i^{ss}_{dc}(t_2)$	$i^{ts}_{dc}(t_1)$	$i^{ts}_{dc}(t_2)$	Δi_{dc}	Err_i
Sub1	2199	2165	2199	2145	-34	20
Sub2	1054	527	1054	443	-527	84
Sub3	3817	-1526	3817	-1318	-5343	-208
Sub4	326	373	326	270	47	103
Sub5	847	1091	847	1029	244	62
Sub6	-2240	-2251	-2240	-2190	-10	-61
Sum	6003	379	6003	379	-5624	0

Figure 25 shows the diagram of simulation results comparison between steady-state simulation and transient-state simulation. It can be more clearly seen from Figure 25 that the deviation value Err_i of a substation at t_2 are related to that of the adjacent substations. Due to the power balance between the substations and the trains in the RTPSS, a large Err_i of a substation could lead to relatively large Err_i with opposite sign in the adjacent substation, for example the Sub4 in the time interval [3025, 3026] and Sub3 in the time interval [3075, 3076]. This also means that the power distribution among the reversible substations has not reached the steady-state at this moment. This phenomenon is in accordance with the actual situation. The proposed hybrid simulation is able to describe accurate operation states of RTPSSs with controllable converters.

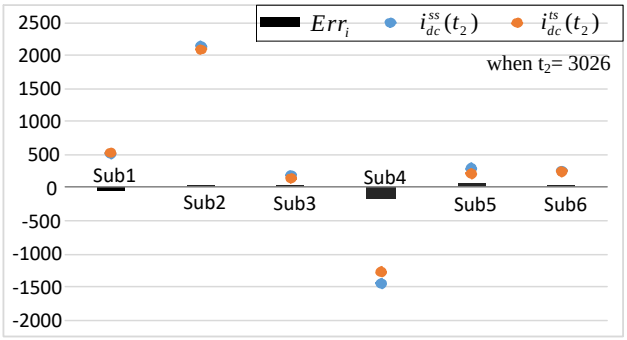

(a)

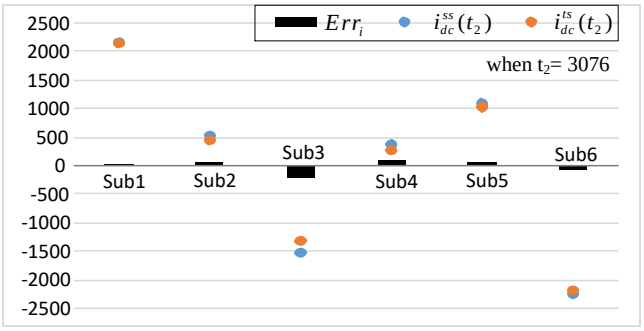

(b)

Figure 25 Diagram of simulation results comparison

5 Conclusion

In the paper, the RTPSS based on 4QC has been recommended as a comprehensive solution for DC railway to improve regenerative braking energy recovery, DC voltage regulation, reactive power compensation, and catenary deicing. In order to undertake a systematic study of the RTPSS, a novel hybrid simulation method integrating train motion, steady-state and transient-state model has been proposed. The structure and signal flow of the hybrid simulation system has been introduced and the methodology of modeling has been presented in details. The train motion simulation has been used to provide the position and the power of each train. The steady-state simulation has provided voltage, current, power and energy for the analysis at system-level, and also to provide the initial values of the state variables for the transient-state simulation. The transient-state simulation has been then carried out to verify the control strategy and parameters. The performance of RTPSS with multiple trains has been evaluated using the proposed hybrid simulation method for a case study of a 10 km railway line with 6 reversible substations and a headway between the trains of 120 seconds. The methodology can reduce the time of simulations without reducing the accuracy of the results, and can be also applied to other power supply systems that include components operating with significantly different time constants.

Acknowledgments: The work was supported by the National Key Research and Development Program [Grant NO.2017YFB1200802]; and the Beijing Science and Technology project [Grant NO. Z171100002217025].

Reference

[1] R. Liu, W. Liu, H. Cui, J. Zhang, and J. Liao, "Capacity optimization design of reactive compensation device in urban rail traction power supply system," in *2017 IEEE Transportation Electrification Conference and Expo, Asia-Pacific (ITEC Asia-Pacific)*, 2017, pp. 1-6.

[2] S. Reza, M. Azah and H. Shareef, "Comparative study of effectiveness of different var compensation devices in large-scale power networks," *Journal of Central South University*, vol. 03, pp. 715-723, 2013.

[3] T. Suzuki, "DC power-supply system with inverting substations for traction systems using regenerative brakes," *IEE Proceedings B - Electric Power Applications*, vol. 129, pp. 18-26, 1982.

[4] B. Mellitt, Z. S. Mouneimne and C. J. Goodman, "Simulation study of DC transit systems with inverting substations," *IEE Proceedings B - Electric Power Applications*, vol. 131, pp. 38-50, 1984.

[5] S. T. Yii, W. Ruay-Nan and C. Nanming, "Electric network solutions of DC transit systems with inverting substations," IEEE Transactions on Vehicular Technology, vol. 47, pp. 1405-1412, 1998.

[6] H. Douglas, C. Roberts, S. Hillmansen, and F. Schmid, "An assessment of available measures to reduce traction energy use in railway networks," Energy Conversion and Management, vol. 106, pp. 1149-1165, 2015.

[7] A. González-Gil, R. Palacin and P. Batty, "Sustainable urban rail systems: Strategies and technologies for optimal management of regenerative braking energy," Energy Conversion and Management, vol. 75, pp. 374-388, 2013.

[8] V. Gelman, "Braking energy recuperation," IEEE Vehicular Technology Magazine, vol. 4, pp. 82-89, 2009.

[9] D. Cornic, "Efficient recovery of braking energy through a reversible dc substation," in Electrical Systems for Aircraft, Railway and Ship Propulsion, 2010, pp. 1-9.

[10] H. Ibaiondo and A. Romo, "Kinetic energy recovery on railway systems with feedback to the grid," in Proceedings of 14th International Power Electronics and Motion Control Conference EPE-PEMC 2010, pp. T9-94-T9-97.

[11] J. Nomura, A. Kataoka and K. Inagaki, "Development of a Hybrid Inverter and a Hybrid Converter for an electric railway," in 2007 Power Conversion Conference - Nagoya, 2007, pp. 1164-1169.

[12] W. A. G. De Jager, "Buddy bidirectional supply for traction substations," in Proceedings of the 2011 14th European Conference on Power Electronics and Applications, 2011, pp. 1-10.

[13] M. Popescu, A. Bitoleanu, V. Suru, and A. Preda, "System for converting the DC traction substations into active substations," in 2015 9th International Symposium on Advanced Topics in Electrical Engineering (ATEE), 2015, pp. 632-637.

[14] C. V. Suru, M. Popescu and A. Bitoleanu, "Control algorithm implementation for a filtering and regeneration system used in urban traction DC substations," in 2016 International Symposium on Power Electronics, Electrical Drives, Automation and Motion (SPEEDAM), 2016, pp. 651-656.

[15] A. Bitoleanu, M. Popescu and C. V. Suru, "Theoretical and experimental evaluation of the indirect current control in active filtering and regeneration systems," in 2017 International Conference on Optimization of Electrical and Electronic Equipment (OPTIM) & 2017 Intl Aegean Conference on Electrical Machines and Power Electronics (ACEMP), 2017, pp. 759-764.

[16] M. Popescu, A. Bitoleanu and M. Dobriceanu, "FBD-based control in active DC-traction substations," in 2016 International Conference on Applied and Theoretical Electricity (ICATE), 2016, pp. 1-6.

[17] V. Gelman, "Energy Storage That May Be Too Good to Be True: Comparison Between Wayside Storage and Reversible Thyristor Controlled Rectifiers for Heavy Rail," IEEE Vehicular Technology Magazine, vol. 8, pp. 70-80, 2013.

[18] N. Ghaviha, J. Campillo, M. Bohlin, and E. Dahlquist, "Review of Application of Energy Storage Devices in Railway Transportation," Energy Procedia, vol. 105, pp. 4561-4568, 2017.

[19] T. Ratniyomchai, S. Hillmansen and P. Tricoli, "Recent developments and applications of energy storage devices in electrified railways," IET Electrical Systems in Transportation, vol. 4, pp. 9-20, 2014.

[20] P. Arboleya, B. Mohamed and I. El-Sayed, "DC railway simulation including controllable power electronic and energy storage devices," IEEE Transactions on Power Systems, p.1-1, 2017.

[21] D. Iannuzzi, D. Lauria and P. Tricoli, "Optimal design of stationary supercapacitors storage devices for light electrical transportation systems," Optimization and Engineering, vol. 13, pp. 1-16, 2012.

[22] K. Itani, A. De Bernardinis, Z. Khatir, A. Jammal, and M. Oueidat, "Extreme conditions regenerative braking modeling, control and simulation of a hybrid energy storage system for an electric vehicle," in IEEE Transactions on Transportation Electrification. vol. PP, 2016, p. 1-1.

[23] M. L. Pastor, L. G. T. Rodriguez and C. V. Velez, "Flywheels Store to Save: Improving railway efficiency with energy storage.,". vol. 1, 2013, pp. 13-20.

[24] A. M. Gee and R. W. Dunn, "Analysis of Trackside Flywheel Energy Storage in Light Rail Systems," IEEE Transactions on Vehicular Technology, vol. 64, pp. 3858-3869, 2015.

[25] D. Roch-Dupré, Á. J. López-López, R. R. Pecharromán, A. P. Cucala, and A. Fernández-Cardador, "Analysis of the demand charge in DC railway systems and reduction of its economic impact with Energy Storage Systems," International Journal of Electrical Power & Energy Systems, vol. 93, pp. 459-467, 2017.

[26] T. Rekha and A. B. Beevi, "Power quality control in DC traction systems using static var compensator and harmonic filter," *International Journal of Engineering Research & Technology*, vol. 3, pp. 733-740, 2014.

[27] J. Wang, "Discussion on Application of Dynamic Reactive Power Compensation Device SVG in Subway Power Supply System,". vol. 12, 2013, pp. 101-107.

[28] Z. Zhu, "Research on Reactive Power Compensation Scheme and Compensation Capacity of Subway Power Supply System," *The World of Inverters*, vol. 11, pp. 45-47, 2014.

[29] G. Zhang, J. Qian and X. Zhang, "Application of a High-Power Reversible Converter in a Hybrid Traction Power Supply System," Applied Sciences, vol. 7, p. 282, 2017.

[30] X. Zhang, P. Chen, C. Yu, F. Li, H. T. Do, and R. Cao, "Study of a Current Control Strategy Based on Multisampling for High-Power Grid-Connected Inverters With an LCL filter," IEEE Transactions on Power Electronics, vol. 32, pp. 5023-5034, 2017.

[31] C. Mayet, P. Delarue, A. Bouscayrol, E. Chattot, and J. N. Verhille, "Comparison of Different EMR-Based Models of Traction Power

Substations for Energetic Studies of Subway Lines," IEEE Transactions on Vehicular Technology, vol. 65, pp. 1021-1029, 2016.
[32] C. Mayet, L. Horrein, A. Bouscayrol, P. Delarue, J. N. Verhille, E. Chattot, and B. Lemaire-Semail, "Comparison of Different Models and Simulation Approaches for the Energetic Study of a Subway," IEEE Transactions on Vehicular Technology, vol. 63, pp. 556-565, 2014.
[33] N. Zhao, C. Roberts, S. Hillmansen, Z. Tian, P. Weston, and L. Chen, "An integrated metro operation optimization to minimize energy consumption," Transportation Research Part C: Emerging Technologies, vol. 75, pp. 168-182, 2017.
[34] S. S., T. T. and R. C., "A Cooperative Train Control Model for Energy Saving," IEEE Transactions on Intelligent Transportation Systems, vol. 16, pp. 622-631, 2015.
[35] P. Arboleya, G. Diaz and M. Coto, "Unified AC/DC Power Flow for Traction Systems: A New Concept," IEEE Transactions on Vehicular Technology, vol. 61, pp. 2421-2430, 2012.
[36] M. Coto, P. Arboleya and C. Gonzalez-Moran, Optimization approach to unified AC/DC power flow applied to traction systems with catenary voltage constraints vol. 53, 2013.
[37] T. Xin, C. Roberts, J. He, S. Hillmansen, N. Zhao, L. Chen, Z. Tian, and S. Su, "Railway vertical alignment optimisation at stations to minimise energy," in 17th International IEEE Conference on Intelligent Transportation Systems (ITSC), 2014, pp. 2119-2124.
[38] Z. Tian, S. Hillmansen, C. Roberts, and P. Weston, "Energy evaluation of the power network of a DC railway system with regenerating trains," Iet Electrical Systems in Transportation, vol. 6, pp. 41-49, 2015.
[39] Z. Tian, S. Hillmansen, C. Roberts, P. Weston, L. Chen, N. Zhao, S. Su, and T. Xin, "Modeling and simulation of DC rail traction systems for energy saving," in 17th International IEEE Conference on Intelligent Transportation Systems (ITSC), 2014, pp. 2354-2359.
[40] Z. Tian, P. Weston, N. Zhao, S. Hillmansen, C. Roberts, and L. Chen, "System energy optimisation strategies for metros with regeneration," Transportation Research Part C: Emerging Technologies, vol. 75, pp. 120-135, 2017.
[41] R. A. Jabr and I. Džafić, "Solution of DC Railway Traction Power Flow Systems Including Limited Network Receptivity," IEEE Transactions on Power Systems, vol. 33, pp. 962-969, 2018.
[42] C. H. Bae, M. S. Han, Y. K. Kim, C. Y. Choi, and S. J. Jang, "Simulation Study of Regenerative Inverter for DC Traction Substation," in 2005 International Conference on Electrical Machines and Systems, 2005, pp. 1452-1456.
[43] W. Kong, L. Qin, Q. Yang, and F. Ding, "DC side short circuit transient simulation of DC traction power supply system," in International Conference on Power System Technology, 2004, pp. 182-186.
[44] BS EN 50163-2004 Railway Applications - Supply Voltages of Traction Systems.
[45] M. W., R. C. and H. S., "Modelling of AC feeding systems of electric railways based on a uniform multi-conductor chain circuit topology," in IET Conference on Railway Traction Systems (RTS 2010), 2010, pp. 1-5.